



NRL/MR/6410--98-8159

Numerical Modeling of Fire Suppression Using Water Mist. 2. An Optimization Study on Jet Diffusion Flames

K. PRASAD

*Science Application International Corporation
Virginia*

C. LI

K. KAILASANATH

*Center for Reactive Flow and Dynamical Systems
Laboratory for Computational Physics and Fluid Dynamics*

June 22, 1998

19980717 019

Approved for public release; distribution is unlimited.

REPRODUCTION QUALITY NOTICE

This document is the best quality available. The copy furnished to DTIC contained pages that may have the following quality problems:

- **Pages smaller or larger than normal.**
- **Pages with background color or light colored printing.**
- **Pages with small type or poor printing; and or**
- **Pages with continuous tone material or color photographs.**

Due to various output media available these conditions may or may not cause poor legibility in the microfiche or hardcopy output you receive.



If this block is checked, the copy furnished to DTIC contained pages with color printing, that when reproduced in Black and White, may change detail of the original copy.

REPORT DOCUMENTATION PAGE

Form Approved
OMB No. 0704-0188

Public reporting burden for this collection of information is estimated to average 1 hour per response, including the time for reviewing instructions, searching existing data sources, gathering and maintaining the data needed, and completing and reviewing the collection of information. Send comments regarding this burden estimate or any other aspect of this collection of information, including suggestions for reducing this burden, to Washington Headquarters Services, Directorate for Information Operations and Reports, 1215 Jefferson Davis Highway, Suite 1204, Arlington, VA 22202-4302, and to the Office of Management and Budget, Paperwork Reduction Project (0704-0188), Washington, DC 20503.

1. AGENCY USE ONLY (<i>Leave Blank</i>)	2. REPORT DATE June 22, 1998	3. REPORT TYPE AND DATES COVERED NRL Memorandum Report	
4. TITLE AND SUBTITLE Numerical Modeling of Fire Suppression Using Water Mist. 2. An Optimization Study on Jet Diffusion Flames			5. FUNDING NUMBERS PE - 62121NPE PR - MA-21-3-01
6. AUTHOR(S) K. Prasad,* C. Li, and K. Kailasanath			
7. PERFORMING ORGANIZATION NAME(S) AND ADDRESS(ES) Naval Research Laboratory Washington, DC 20375-5320			8. PERFORMING ORGANIZATION REPORT NUMBER NRL/MR/6410--98-8159
9. SPONSORING/MONITORING AGENCY NAME(S) AND ADDRESS(ES) Office of Naval Research Arlington, VA 22217			10. SPONSORING/MONITORING AGENCY REPORT NUMBER
11. SUPPLEMENTARY NOTES *Science Application International Corporation, VA			
12a. DISTRIBUTION/AVAILABILITY STATEMENT Approved for public release; distribution unlimited.			12b. DISTRIBUTION CODE
13. ABSTRACT (<i>Maximum 200 words</i>) This report is the second in a series that discusses the numerical modeling of fire suppression using water-mist. In the first report, a numerical study was described for obtaining a detail understanding of the physical processes involved during the interaction of water-mist and flames. The relative contribution of the various suppression mechanisms for methane-air diffusion flames was studied and detailed comparison with experimental results was provided in the first report. The present report describes a computational study for optimizing water-mist injection characteristics for suppression of co-flow diffusion flames. A two-continuum formulation is used in which the gas phase and the water-mist are both described by equations of the Eulerian form. Numerical simulations are performed to optimize various water-mist injection characteristics for maximum flame suppression. The effects of droplet diameter, mist in injection angle (throw angle), mist density and velocity on water-mist entrainment into the flame and flame suppression are quantified. Droplet sectional trajectories and density contours are used to identify the regions of the flame where the droplets evaporate and absorb energy. Numerical results are presented for symmetric and asymmetric spray pattern geometries resulting from base injection and side injection nozzle orientation. Results indicate that smaller droplet diameters produce optimum suppression under base injection configuration, while larger droplet diameters are needed for optimum suppression for the side injection configuration. For all cases, the model is used to determine the water-mist required for extinction, and this is reported in terms of the ratio of the water supply rate to the fuel flow rate.			
14. SUBJECT TERMS Fire suppression Diffusion flame Water mist Numerical modeling			15. NUMBER OF PAGES 26
			16. PRICE CODE
17. SECURITY CLASSIFICATION OF REPORT UNCLASSIFIED	18. SECURITY CLASSIFICATION OF THIS PAGE UNCLASSIFIED	19. SECURITY CLASSIFICATION OF ABSTRACT UNCLASSIFIED	20. LIMITATION OF ABSTRACT UL

CONTENTS

1. INTRODUCTION	1
2. PROBLEM FORMULATION	2
2.1 Gas Phase Equations	2
2.2 Sectional Water Mist Model	4
2.3 Numerical Algorithm	5
3. RESULTS AND DISCUSSION	6
3.1 Base Injection Configuration - Co-flow Injection	6
3.2 Symmetric/Asymmetric Injection Configuration	7
3.3 Base Injection Configuration - Angle Injection	8
3.4 Side Injection Configuration	9
3.5 Top Injection Configuration	10
4. CONCLUSIONS	10
5. ACKNOWLEDGEMENT	11
6. REFERENCES	12

LIST OF FIGURES

1	Schematic diagram of a 2-Dimensional diffusion flame burner and the associated computational domain in which the solutions are desired. The figure also shows the various water-mist injection configurations that are studied in this report.	13
2	The effect of droplet injection diameter and injection velocity on overall flame suppression is shown as a function of mist to fuel flow rate. The arrows in the insert indicate the direction in which water-mist is injected.	14
3	The effect of droplet injection density and spray pattern (symmetric or asymmetric injection) on overall flame suppression shown as a function of mist to fuel flow rate. The arrows in the inserts indicate the direction in which water-mist is injected. . .	14
4	The effect of varying the mist injection velocity on the temperature distribution for asymmetric mist injection at 45° angle to the air co-flow. The initial droplet diameter is 50μ and the injection density is $1000\text{drops}/\text{cm}^3$. The mist injection velocity is varied from $0.25\text{m}/\text{s}$ to $2.25\text{m}/\text{s}$	15
5	Velocity vectors and streamline pattern during symmetric injection of water-mist at 45° angle to the air co-flow. The mist injection velocity is varied 0.25 m/s (top) to 2.25 m/s (bottom).	16
6	Temperature contours for the asymmetric injection configuration of water-mist at 45° angle to the air co-flow. The water-mist droplet diameter is 50μ and the injection density is $4000\text{ drops}/\text{cm}^3$. The mist injection velocity is varied from $1.75\text{m}/\text{s}$ to $7.00\text{m}/\text{s}$	17
7	Sectional density contours above a methane-air diffusion flame burner for asymmetrical injection of water-mist at 45° angle. The water-mist droplet diameter is 50μ , injection density is $4000\text{ drops}/\text{cm}^3$ and mist injection velocity is $1.75\text{m}/\text{s}$	18
8	Net suppression effect of water-mist as a function of injection angle. Both symmetric and asymmetric base injection configurations are considered.	18
9	Temperature contours during symmetric injection configuration of water-mist at various injection angles. Droplet diameter is 150μ , injection density = $100\text{ drop}/\text{cm}^3$ and injection velocity = $1.00\text{m}/\text{s}$	19
10	Heat release rate contours ($\text{J}/\text{m}^3/\text{s}$) during side injection of water-mist. Figure shows the exothermic contours (red) at the flame sheet due to oxidation of the fuel molecule, and endothermic contours (blue) due to evaporation of water droplets. . .	19
11	Velocity vectors (m/s) superimposed on temperature (K) distributions during side injection of water-mist into a methane-air diffusion flame.	20
12	Sectional density contours above a methane-air diffusion flame burner for side injection of water-mist. The water-mist droplet diameter is 50μ , injection density is $2000\text{ drops}/\text{cm}^3$ and mist injection velocity is $12.5\text{m}/\text{s}$	20
13	Net suppression effect of water-mist as a function of mist to fuel flow rate ratio for side injection configuration. The effect of droplet diameter on overall flame suppression has been shown for (asymmetric) diffusion flames. The arrows in the insert indicate the direction in which water-mist is injected.	21
14	Net suppression effect of water-mist as a function of mist to fuel flow rate ratio for various injection configuration and spray pattern geometries.	22

Numerical Modeling of Fire Suppression using Water Mist. 2. An Optimization Study on Jet Diffusion Flames

1. INTRODUCTION

Water as a means of fire suppression has been in use from ancient times. The phase-out of halons and the search for alternative technologies that preserve all of the benefits of a clean total flooding agent without the adverse environmental impact has sparked renewed interest in water-mist technology. Fine water-mist relies on relatively small (less than $200 \mu m$) "Class 1" droplet sprays to extinguish fires. Although the usefulness of water-mist fire suppression systems has been demonstrated in a wide range of applications and by numerous experimental programs (References [1]- [9]), a widely accepted critical concentration of water droplets required to extinguish a fire is yet to be determined. Factors that contribute to the success or failure of a water-mist system for a particular application include droplet size, velocity, spray pattern geometry, nozzle orientation, momentum and mixing characteristics of the spray jet, geometry and other characteristics of the protected area. At this time the effect of these factors on system effectiveness is not well known. There is no current theoretical basis for the selection of spray characteristics and other important water-mist system parameters.

Extinguishment of jet diffusion flames by the introduction of water sprays at the base of the flame has been studied by a number of investigators [1]- [4]. These flames can be extinguished very efficiently by this technique since the normal air entrainment process assures that all the water spray added adjacent to the flame is actually transported into the flame. The water required for extinguishment is reported in terms of the ratio of the water supply rate to the fuel supply rate at extinction. These ratios range from 1.5 to 10. While no systematic evaluation of droplet sizes on the water/fuel ratio at extinction has been performed, the available data indicate that the ratio is reduced with decreasing droplet size for laboratory flames. Large scale flames could be extinguished with a water/fuel ratio of 1.6. However, ratios of up to 10 may be required depending on the orientation and geometry of the spray nozzles.

The available research in water spray fire extinguishment was reviewed by McCaffrey [2], Rashbash [5] and by Tatem et al. [6]. McCaffrey [2] has reviewed the available data for the application of water sprays as a jet diffusion flame suppression/extinguishment agent. Reduction in flame temperature during sub-extinguishing application rates of water spray has been observed to correlate with a single spray parameter - the median drop diameter. The effect of adding water spray to the gas flow below the base of a lifted flame is to change the flame shape and to lower peak flame temperature and radiation levels. Extinguishment near blow-off was observed to be due to a shift in flame position [2]. The influence of droplet diameter, density and velocity on flame suppression for various nozzle orientations and spray pattern geometries has not been reported in a detailed parametric fashion in the literature.

There has been some theoretical and experimental work ([10]- [15]) to develop an understanding of gas phase extinguishment of fires. Numerical studies for a counterflow methane/air diffusion flame with heptane droplets added to the fuel stream have been reported by Chen et al. [14]. Atreya [15] has observed enhancement of the burning rate at low water addition rates followed by flame extinguishment at higher application rates for counterflow diffusion flames. Mawhinney et al. [3] has also reported evidence of invigoration of combustion by the introduction of water-mist. The time to extinguish a fire was reported as a function of fuel type, geometry and mist characteristics. Hoffman and Galea [16], [17] have used the field modeling technique to include two-phase fire-sprinkler scenarios. In these studies the fire is seen simply as a heat source without the added complication of combustion. The model results are compared with experimental data and shows good agreement near the sprinkler source, but deteriorates in the far field. More recently, Prasad et al. [18], [19] have studied the relative contribution of various flame suppression mechanisms (thermal cooling and oxygen dilution), and have made detailed comparisons with experimental results.

The overall objective of this study is to develop and apply a numerical model for studying the underlying processes involved in suppression of fires with water-mist. Overall flame suppression and mist entrainment into the flame and their dependence on droplet diameter, spray velocity and injection characteristics (orientation of the nozzles relative to the flame and angle of injection) is determined. Sectional trajectories are used to identify the regions of the flame (preheat zone, combustion zone or plume zone) where the droplets evaporate and absorb energy. Numerical simulations are performed for both symmetric and asymmetric spray injection geometries (base injection or side injection). In this report, "Flame Suppression" is used to indicate a reduction in the net heat output from a flame. The water-mist required for different levels of suppression is reported in terms of the ratio of water-mist flow rate to the fuel flow rate. This ratio is related to the water-mist loading which is simply the ratio of water-mist flow rate to the air flow rate. The goal of the current work is not to optimize the design of water-mist systems, but to determine the optimum injection characteristics of a water-mist system to suppress a specific fire - a jet diffusion flame. Several such fire science studies are needed before arriving at the optimum characteristics for any arbitrary fire. Additional system configuration studies will be needed to determine the optimum placement of water-mist systems for suppression of fires in a specific enclosure.

2. PROBLEM FORMULATION

We consider the interaction of fine water-mist with methane-air diffusion flames stabilized above a Wolfhard-Parker burner geometry. There are two interacting physical phases, the gas phase involving convection, diffusion and chemical reactions between the constituent species, and the liquid phase, representing the evaporating water droplets. A two-continuum formulation is adopted in which gas properties and the droplet properties are each described by equations of the Eulerian form.

2.1 Gas Phase Equations

Detailed modeling of gas-phase reactive flows is based on a generally accepted set of time-dependent coupled partial differential equations maintaining conservation of total mass, momentum, total energy and individual species density. A strong conservation form of the two-dimensional, unsteady, compressible Navier-Stokes equations, used to describe gas phase reactive flow systems can be written as follows [18]

$$\frac{\partial \rho}{\partial t} + \frac{\partial \rho u}{\partial x} + \frac{\partial \rho v}{\partial y} = \dot{m}_{evap}, \quad (1)$$

$$\frac{\partial(\rho u)}{\partial t} + \frac{\partial(\rho u^2 + P)}{\partial x} + \frac{\partial(\rho uv)}{\partial y} = \frac{\partial \tau_{xx}}{\partial x} + \frac{\partial \tau_{xy}}{\partial y} + \dot{S}_x, \quad (2)$$

$$\frac{\partial(\rho v)}{\partial t} + \frac{\partial(\rho uv)}{\partial x} + \frac{\partial(\rho v^2 + P)}{\partial y} = \frac{\partial \tau_{yx}}{\partial x} + \frac{\partial \tau_{yy}}{\partial y} - \rho g + \dot{S}_y, \quad (3)$$

$$\begin{aligned} \frac{\partial(\rho E)}{\partial t} + \frac{\partial((\rho E + P)u)}{\partial x} + \frac{\partial((\rho E + P)v)}{\partial y} &= \frac{\partial(\tau_{xx}u)}{\partial x} + \frac{\partial(\tau_{xy}u)}{\partial y} + \frac{\partial(\tau_{yx}v)}{\partial x} + \frac{\partial(\tau_{yy}v)}{\partial y} \\ &+ \frac{\partial q_x}{\partial x} + \frac{\partial q_y}{\partial y} - \rho g v + Q_{chem} + Q_{rad} + Q_{evap}, \end{aligned} \quad (4)$$

$$\frac{\partial \rho_k}{\partial t} + \frac{\partial(\rho_k u)}{\partial x} + \frac{\partial(\rho_k v)}{\partial y} = -\frac{\partial(\rho_k U_k)}{\partial x} - \frac{\partial(\rho_k V_k)}{\partial y} + \dot{m}_{k,evap} + \dot{\omega}_k, \quad k = 1, 2, \dots, N. \quad (5)$$

In these equations x and y denote the independent spatial coordinate and t denotes the temporal coordinate; ρ the mass density; ρ_k the density of the k^{th} species; u and v are the x and y components of the fluid bulk velocity; P , the pressure; E , the total energy of the fluid per unit mass; g , the gravitational body force per unit mass; U_k and V_k are the two components of the diffusion velocity for the k^{th} species; τ_{xx} , τ_{xy} , τ_{yy} are the components of the stress tensor for newtonian fluid in rectangular coordinate; q_x and q_y are the x and y components of the heat-flux vector. \dot{m}_{evap} is the source term arising in the mass conservation equation due to evaporation of the water droplets, resulting in the production of water vapor. The corresponding term in the water vapor species conservation equation is represented by $\dot{m}_{k,evap}$. $\dot{\omega}_k$ is the rate of production of the k^{th} species due to chemical reactions. Q_{chem} is an exothermic source term in the energy equation representing chemical energy release, whereas Q_{evap} represents absorption of energy due to droplet evaporation; Q_{rad} is the radiative heat loss term. \dot{S}_x and \dot{S}_y are the source terms in the x and y momentum equations representing the cumulative drag force exerted by the droplets on the gas phase.

Ideally, we would like to simulate the chemical reactions by including a detailed set of elementary reactions to describe the production of the individual species and the energy release in the flame. The cost of computer time and memory required to track the individual species makes this prohibitive for problems in which parametric studies are planned. Therefore, the chemical reaction and energy-release process for methane-air combustion is described phenomenologically based on a single step reaction,



using a finite-rate, quasi-global Arrhenius expression. Westbrook et al. [20] has developed simplified reaction mechanisms for the oxidation of hydrocarbons using a laminar flame model and has prescribed an overall rate of consumption of methane as

$$\frac{d[CH_4]}{dt} = -1.3E8 \exp(-48400/RT)[CH_4]^{-0.3}[O_2]^{1.3}. \quad (7)$$

The above expression is used to compute the depletion of methane. The various diffusion coefficients are obtained from detailed kinetic theory and are fitted over a suitable temperature range using a third order polynomial [21].

2.2 Sectional Water Mist Model

In this section the equations describing a vaporizing spray are obtained by a standard control-volume approach. It is assumed that coalescence and breakup of droplets are insignificant within the computational domain. An Eulerian approach is adopted and the droplet properties are treated as if they were continuous in the domain as the gas properties [22], [23]. The vaporization process can be described by a set of coupled differential equations for the concentration n_i of the discrete droplet sizes per unit volume of the fluid,

$$\frac{\partial n_i}{\partial t} + u_{l,i} \frac{\partial n_i}{\partial x} + v_{l,i} \frac{\partial n_i}{\partial y} = -E_i n_i + E_{i+1} n_{i+1}, \quad i = 1, 2, \dots, \quad (8)$$

where $u_{l,i}$ and $v_{l,i}$ are the x and y components of the velocity vector of the i^{th} droplet size and E_i is the frequency of the molecule evaporation. This frequency appearing in the discrete form of the droplet population balance equations, depends on surface area of the droplet, temperature of the ambient gas and other flow parameters. Functional forms of this frequency can be obtained through known expressions of vaporization rates of single droplets or may be determined through correlations with known experimental results of measured vaporization rates. Since the total number of droplet sizes needed to simulate actual fuel sprays can be immense, sectional conservation equations have been employed [24]. The method of "section conservation" avoids the dimensionality problem associated with the discrete form of the droplet population balance equations 8. This method is based on dividing the droplet size domain into sections and dealing only with one integral quantity in each section. This sectional representation has the advantage that the integral quantity is conserved within the computational domain and the number of conservation equations is substantially reduced so as to equal the number of sections.

We divide the entire droplet size domain into M arbitrary sections, and define Q_j to be an integral quantity of the spray within the j^{th} section. Thus

$$Q_j = \int_{v_{j-1}}^{v_j} v n dv, \quad j = 1, 2, \dots, M, \quad (9)$$

where $n(v, t)$ is the number concentration function and v_{j-1} and v_j denote the volumes of the smallest and largest droplets, respectively, in section j . The quantity Q_j can be related to volume or the mass of the droplets within the j^{th} section. Using equations 8 and 9, the sectional conservation equation can be written as

$$\frac{\partial Q_j}{\partial t} + u_{l,j} \frac{\partial Q_j}{\partial x} + v_{l,j} \frac{\partial Q_j}{\partial y} = -C_j Q_j + B_{j,j+1} Q_{j+1}, \quad j = 1, 2, \dots, M, \quad (10)$$

where $B_{j,j+1}$ and C_j are the sectional coefficients. Assuming a d^2 law to re-express the sectional vaporization coefficients in terms of droplet diameters [18] and assuming a continuous division into sections the coefficients can be expressed as

$$B_{j,j+1} = \frac{3}{2} E(T) \left[\frac{d_{L,j+1}}{d_{U,j+1}^3 - d_{L,j+1}^3} \right], \quad j = 1, 2, \dots, M-1, \\ C_j = \frac{3}{2} E(T) \left[\frac{d_{L,j}}{d_{U,j}^3 - d_{L,j}^3} - \frac{3(d_{U,j} - d_{L,j})}{d_{U,j}^3 - d_{L,j}^3} \right], \quad j = 1, 2, \dots, M, \quad (11)$$

where $E(T)$ is the burning rate coefficient, which depends on temperature and other properties of the droplet and its surroundings. For example, with an initial injection droplet diameter of 150μ , the droplet size domain is divided into 5 continuous division ($M = 5$). These sections are $0 - 30\mu m$, $30 - 60\mu m$, $60 - 90\mu m$, $90 - 120\mu m$ and $120 - 150\mu m$.

Each of the droplet sections is assumed to have its own unique velocity different from that of the gas phase. Momentum conservation equations are formulated for each droplet section and are coupled to those of the gas phase through the phase interaction terms (drag terms). The droplet drag equations are given by

$$\begin{aligned} \frac{\partial u_{i,j}}{\partial t} + u_{i,j} \frac{\partial u_{i,j}}{\partial x} + v_{i,j} \frac{\partial u_{i,j}}{\partial y} &= F_{x,j}, \quad j = 1, 2, \dots, M, \\ \frac{\partial v_{i,j}}{\partial t} + u_{i,j} \frac{\partial v_{i,j}}{\partial x} + v_{i,j} \frac{\partial v_{i,j}}{\partial y} &= F_{y,j} - g, \quad j = 1, 2, \dots, M, \end{aligned} \quad (12)$$

where $F_{x,j}$ and $F_{y,j}$ are the x and y components of the drag force acting on the j^{th} sectional velocity modeled based on Stokes Law. The interphase drag force experienced by the two phases is related to the particle Reynolds number by a drag coefficient C_D . The gas phase momentum source terms \dot{S}_x and \dot{S}_y are equal and opposite to the sectional density weighted sum of $F_{x,j}$ and $F_{y,j}$ respectively [18], [25].

2.3 Numerical Algorithm

The governing equations are rewritten in terms of finite-volume approximations on an Eulerian mesh and solved numerically using a time marching procedure. The fluid convection is solved with a high-order implicit algorithm, Barely Implicit Correction to the Flux-Corrected Transport (BIC-FCT) [26], that was developed to solve the convection equations for low-velocity flows. The Flux-Corrected Transport (FCT) [27] algorithm itself is an explicit, finite-difference algorithm that is constructed to have fourth-order phase accuracy. The solution approach consists of separate algorithms for each of the individual processes, which are coupled together by the method of fractional time-step splitting. The algorithms for convection, thermal conduction, molecular diffusion, chemical reactions and the coupling of the individual processes have been previously discussed in detail [26].

Figure 1 shows a schematic diagram of a 2-Dimensional Wolfhard-Parker diffusion flame burner along with the associated computational domain in which the solutions are desired. The various water-mist injection configurations such as base injection, side injection and top injection used in this optimization study have also been illustrated. A specific solution of the reactive flow equations is determined by the initial and boundary conditions that describe the geometry of the system and exchange of mass, momentum and energy occurring between the system and the rest of the physical world. The various species densities and jet velocities are prescribed at the inflow boundary. At the outflow boundary, the normal gradients of total density, species densities and momentum was assumed to be zero. The pressure at large distances from the burner surface is assumed to be equal to the ambient pressure. Symmetric boundary condition was employed at the center line of the computational domain by use of anti-symmetric reflection of tangential velocity v , and symmetric reflection of all other variables. A slip wall boundary condition is employed at the lateral boundary by assuming that the flux of all transported properties across the wall is zero. For asymmetric flame calculation slip wall boundary conditions are invoked at both lateral boundaries.

The computational domain for a symmetric calculation consists of a stretched 96×128 grid, concentrated near the contact point of the fuel and the oxidizer. The smallest grid cell is a $0.5\text{mm} \times 0.5\text{mm}$ square cell. Numerical simulations were performed by halving the grid size to check for accuracy and consistency. The algorithms have been optimized for efficient performance on vector machines. Typical computational time on a C-90 single processor machine was approximately 4 hours to reach a steady state solution.

3. RESULTS AND DISCUSSION

The governing equations described earlier were solved using the numerical models briefly discussed above, to simulate co-flow methane-air diffusion flames stabilized above a Wolfhard Parker burner. Computations were performed to study the interaction of water-mist and the diffusion flame for various droplet diameters, spray injection density, velocity and injection configurations (side injection or base injection, symmetric or asymmetric spray pattern geometry). Simulations were performed to estimate the impact of various injection configurations on overall flame suppression, flame structure and flow pattern.

First, numerical simulations were performed for the base case methane-air diffusion flame (without any injection of water-mist). The average exit velocity of fuel jet (CH_4) was 2.81 cm/s and the average exit velocity of the air jet was 18.1 cm/s (See Figure 1). Temperature profiles at various heights above the burner surface were compared with experimental data obtained over a similar geometry. At each height the numerically computed temperature profiles compared favorably with the thermocouple temperature measurements [18], indicating that the exothermic chemical reactions and energy release are adequately modeled by the single step Arrhenius reaction mechanism. Numerical calculations and temperature measurements were performed for various nitrogen dilution levels on methane-air diffusion flames to study the impact of oxygen displacement. Numerically computed temperature profiles again compared favorably with experimental results at various heights above the burner surface [18], [19].

3.1 Base Injection Configuration - Co-flow Injection

With the confidence gained by the comparison with experimental data, a series of numerical simulations were performed to determine the underlying processes involved in suppression of flames with water-mist. Water-mist is introduced along with the air co-flow at the base of the diffusion flame (base injection). Parametric studies were performed with $50\mu\text{m}$ droplets injected uniformly over the length of the air channel with spray injection density varying from 1000 drop/cm^3 (0.065kg/m^3) to 4000 drop/cm^3 and injection velocity varying from 25 cm/s to 100 cm/s . Similar studies were performed for $100\mu\text{m}$ and $150\mu\text{m}$ monodisperse droplets with injection density varying from 50 drop/cm^3 to 1000 drop/cm^3 and mist injection velocity varying over the range of 25 cm/s to 500 cm/s . The temperature and heat release rate profiles indicate an increase in flame height and flame suppression due to the sub-extinguishing application rates of water-mist. The heat release rate profile indicates the presence of an endothermic heat release rate profile (negative value) showing the approximate location of evaporation of the droplets. These profiles along with the section droplet density contours indicate that droplets are unable to cross the flame sheet and enter the diffusion flame.

The net suppression due to water-mist and the impact of droplet diameter, injection velocity and spray density have been summarized in Figure 2. The abscissa shows the net amount of water-

mist injected per unit mass flow rate of fuel ($\dot{m}_{mist}/\dot{m}_{fuel}$), whereas the ordinate is a ratio of the integrated heat release in the computational domain with water-mist (ΔH_T) to the integrated value without water-mist (ΔH_o). This ratio therefore represents a net integrated measure of the suppression of a flame. Efficient design of water-mist systems aims at obtaining the maximum amount of suppression (values of $\Delta H_T/\Delta H_o$ close to 0.0) with the minimum amount of water-mist added to system, that is, to minimize the value of the abscissa and the ordinate. Along each curve in Figure 2, droplet diameter and injection velocity is held constant, but spray density is progressively increased resulting in higher mist flow rates. For each droplet diameter, the net suppression increases with spray density. The ratio of mist to fuel flow rate ($\dot{m}_{mist}/\dot{m}_{fuel}$) required for extinction of the diffusion flame is approximately 10 for $50\mu m$ droplets and increases to 40 for $150\mu m$ droplets. Figure 2 also shows cases with three different spray injection velocities ($25cm/s$, $250cm/s$ and $500cm/s$). As the spray velocity increases, we find that net suppression reduces for a given ($\dot{m}_{mist}/\dot{m}_{fuel}$) ratio due to reduced entrainment. Overall our results indicate that for the co-flow configuration, smaller diameter droplets produce maximum suppression for the minimum spray mass density.

3.2 Symmetric/Asymmetric Injection Configuration

Computations were carried out with water-mist injection directed at an angle of 45° to the burner surface for a wide range of droplet diameters, injection densities and spray velocities. Both symmetric and asymmetric spray geometries were considered. Symmetric injection refers to water-mist injection that is directed towards the diffusion flame from both sides of the flame (Figure 3). Under these conditions, the symmetric boundary condition can be invoked at the centerline. Asymmetric injection refers to mist injection directed towards the flame on one side and away from the flame on the other side. Under these conditions the cumulative drag force exerted by the droplets on the gases may be large enough to bend the flame in one direction. Symmetry conditions cannot be invoked at the geometric center line of the system and the entire computational domain has to be solved.

Figure 3 shows the net suppression effect of water-mist due to symmetric and asymmetric injection at 45° angle to the burner surface. Water-mist is injected along with the air co-flow at the base of the diffusion flame (base injection configuration). Along each curve the droplet injection density is kept constant but spray velocity is changed resulting in higher mist flow rates. Results show that for $50\mu m$ droplets under symmetric injection condition, higher injection densities ($2000\text{ drop}/\text{cm}^3$) produce better suppression as compared to lower injection densities ($1000\text{ drop}/\text{cm}^3$). However, asymmetric injection conditions produce lower suppression even with higher mass injection densities ($4000\text{ drop}/\text{cm}^3$) as compared to the symmetric case. During asymmetric water-mist injection, smaller amount of water-mist is entrained into the diffusion flame as compared to the symmetric case resulting in lower suppression. Results also indicate that under asymmetric conditions, $150\mu m$ droplets result in better flame suppression as compared to $50\mu m$ droplets. This result is in contrast with that shown in Figure 2 which shows that smaller droplets produce better flame suppression. In-addition, asymmetric flames require higher $\dot{m}_{mist}/\dot{m}_{fuel}$ ratio for suppression. The temperature and streamline pattern indicate that flame structure and flow field pattern is significantly different between the symmetric and asymmetric configurations.

Temperature contours during symmetric injection of water-mist at 45° angle to the air co-flow have been shown in Figure 4. The mist injection velocity is varied from $0.25m/s$ to $2.25m/s$. The

arrows indicate the initial injection direction at the base of the diffusion flame burner. Results indicate that as the mist velocity increases the flame height (defined as the height above the burner surface along the centerline, where the temperature reaches a local maxima) increases but the maximum temperature decreases. For water-mist injection velocity of 0.25m/s , we observe a peak flame temperature of 1870K and a flame height of 7.0cm . On the other hand for a mist injection velocity of 2.25m/s a peak flame temperature of 1580K was obtained and the corresponding flame height was approximately 10cm . The gas phase velocity vectors (color) and streamline pattern (black) during symmetric injection of water-mist at 45° angle to the air co-flow, for various mist injection velocities has been illustrated in Figure 5. As the mist injection velocity increases, the drag force exerted by the water-mist on the air flow also increases resulting in the bending of the streamlines towards the diffusion flame. The contraction of the streamtube is accompanied with increased entrainment of the air into the diffusion flame. This leads to taller diffusion flames as shown in Figure 4.

The temperature contours during asymmetric injection of water-mist at 45° angle to the air co-flow have been shown in Figure 6. The water-mist droplet diameter is $50\mu\text{m}$ and the injection density is $4000\text{drops}/\text{cm}^3$. The mist injection velocity is varied from 1.75m/s to 7.00m/s . The arrows indicate the initial injection direction of water-mist at the base of the diffusion flame burner. Temperature contours clearly indicate that the diffusion flame bends in the direction of the mist flow. We also observe that the peak temperature increases from 1970K (water-mist injection velocity 1.75m/s) to approximately 2030K for a water-mist injection velocity of 7.00m/s . The large mist injection velocity can significantly alter the air flow patterns resulting in higher peak flame temperatures. Figure 7 shows the sectional density contours above a methane-air diffusion flame burner for asymmetrical injection of water-mist at 45° angle. The sectional density contours indicate the approximate location where the droplets evaporate and absorb energy from the diffusion flame. The asymmetrical sectional density contours for the $0 - 10\mu\text{m}$ and $20 - 30\mu\text{m}$ droplets imply larger extraction of heat on one side of the diffusion flame resulting in asymmetric flames. This explains the observed temperature distribution shown in Figure 6 with one side of the diffusion flame being cooler than the other side.

3.3 Base Injection Configuration - Angle Injection

Figure 8 shows the overall flame suppression as a function of spray injection angle for various spray injection density and velocity. Both symmetric and asymmetric conditions are shown. All the data points on any one curve in Figure 8 have the same ratio of the mist flow rate to fuel flow rate. Hence the use of injection angle as the variable on the abscissa instead of $\dot{m}_{\text{mist}}/\dot{m}_{\text{fuel}}$. Results indicate that for certain conditions the net suppression is independent of the injection angle. When the droplet injection velocity is a close to the gas inlet velocity, the drag force exerted by the gas on the droplets is strong enough to make the water droplets quickly follow the gas phase. As the spray injection velocity increases and becomes significantly different from the gas phase, results indicate an optimum angle for flame suppression. Results for asymmetric injection of mist ($50\mu\text{m}$, density= $1000\text{ drop}/\text{cm}^3$ ($0.065\text{kg}/\text{m}^3$), velocity= 1.75 m/s) show an optimum throw angle of 45° . Similar results were observed for $150\mu\text{m}$ droplets with high injection velocities of 1.0 m/s injected in symmetric or asymmetric manner. Again, as expected, suppression under symmetric conditions was better than under asymmetric conditions for similar injection parameters ($150\mu\text{m}$, density= $100\text{ drop}/\text{cm}^3$ ($0.176\text{kg}/\text{m}^3$), velocity= 1.0 m/s). Figure 9 shows temperature contours during the symmetric injection configuration of water-mist at various injection angles. In these

simulations the droplet diameter is $50\mu m$, injection density is $100\text{drops}/\text{cm}^3$ and injection velocity is $1.00\text{m}/\text{s}$. The maximum temperatures were 1740K , 1720K and 1830K for injection angles of 15° , 45° and 75° respectively.

3.4 Side Injection Configuration

The calculations described thus far (Figures 2-8) are for water-mist injection at the base of the diffusion flame (base injection configuration). We now describe water-mist injection through the side wall. Side injection configuration (see figure 1) are important because they will have a direct influence on the entrainment rate of water-mist into the flame. When water-mist is injected only through one side wall, the cumulative drag force exerted by the droplet sections on the gas phase may result in bending of the diffusion flame due to the cross flow. Figure 10 shows the heat release profiles ($J/\text{m}^3/\text{s}$) during uniform injection of $150\mu m$ droplets distributed evenly through the side wall. The red contours indicate the region of high exothermic chemical activity at the flame sheet. The blue contours mark the location where water droplets evaporate and absorb energy. Unlike the case for base injection of water-mist through the burner surface, results clearly show that water droplets are able to penetrate through the flame sheet and absorb energy inside the flame envelope. Figure 11 shows the gas phase velocity vectors superimposed on temperature contours for the case of side injection of water-mist into a diffusion flame. Results clearly illustrate the bending of the temperature contours representing a diffusion flame stabilized in a mild cross flow. The change in gas phase flow field due to the side injection of water-mist is clearly illustrated by this figure. Sectional density contours (refer Figure 12) also indicate the presence of $0 - 10\mu m$ and $20 - 30\mu m$ droplet sections inside the flame sheet. These contours indicate the locations where water-mist evaporate and absorb energy from the diffusion flame.

Figure 13 shows the net integrated suppression during side injection of water-mist for various injection spray densities and velocities. The effects of droplet diameter on suppression has been shown as a function of mist to fuel flow rate for asymmetric flames. Results clearly show that $150\mu m$ droplets produce more flame suppression as compared to $50\mu m$ droplets for a given $\dot{m}_{mist}/\dot{m}_{fuel}$ ratio. In contrast, base injection configuration show that small droplet diameters ($50\mu m$) suppress flames more than larger droplet diameters ($150\mu m$). The small droplets exhibit small characteristic time for decrease of relative velocity between the gas phase and water droplets. As a result, these droplets quickly follow the gas phase. Larger droplets tend to travel with their injection velocity and exhibit large characteristic time for decrease of relative velocity. When $50\mu m$ drops are injected with moderate injection velocity ($1\text{ m}/\text{s}$) through the side wall, they are unable to cross the width of the air channel and reach the diffusion flame. These droplets are dragged by the air flow out of the computational domain before they reach the flame. Only very high injection velocities ($10\text{ m}/\text{s}$) for the $50\mu m$ droplets are able to reach the diffusion flame. As a result the suppression curve for these drops remains flat (no suppression) for $\dot{m}_{mist}/\dot{m}_{fuel}$ ratio of up to 60. The $150\mu m$ drops are able to cross the width of the air channel, entrain into the diffusion flame and provide flame suppression for smaller injection velocities.

Figure 13 also shows that for the side injection configuration lower spray injection density results in more suppression for a given mist flow rate. This is because to maintain a given mist flow rate, the lower spray density case has a higher mist velocity. Flame suppression increases with higher mist velocity for a given injection density and droplet diameter. On the other hand, as discussed earlier, under the base injection configuration, a higher spray injection density results

in more flame suppression. Flame suppression decreases with higher mist velocity for a given mist flow rate and droplet diameter.

3.5 Top Injection Configuration

Computations were carried out with water-mist injection from the top of the diffusion flame (top injection configuration), as shown in Figure 1. Water-mist was injected through the outflow boundary and directed downwards to the diffusion flame. In the present calculations the outflow boundary was approximately 30cm above the burner surface. Numerical simulations were performed with water-mist injection velocity ranging from 20cm/s to 200cm/s and an initial droplet diameter ranging from 50 μ m to 150 μ m. For small initial injection velocity ranging from 20 – 50cm/s the droplets were unable to overcome the drag force exerted by the hot plume gases. The droplets were observed to quickly reverse their flow direction and convect out of the computational domain along with the gas flow. If the initial injection velocity was greater than 150cm/s, we observed that the droplets were able to change the gas flow field in the plume region. This disturbance of the gases in the plume region resulted in generation of acoustic waves that affected the flame structure. We note that the droplet even for these high injection velocities were unable to reach the diffusion the flame. We conclude that it is difficult for the “Class 1” droplet sprays to penetrate through the plume region and reach the diffusion flame.

Droplets that were injected away from the plume region were also unable to overcome the drag force exerted by the cooler co-flowing air. We note that these droplets travel further down towards the diffusion flame than the droplet that were injected in the plume region. Since the top injection boundary is approximately 30cm above the burner surface, the droplets were unable to come close to the diffusion flame for the injection velocities that we have tested. Simulations are being performed in which the co-flow air velocity is set to zero. Under the condition of zero co-flow air velocity the droplet are able to travel downward under the force of gravity and are able to reach the burner surface. The droplets were found to entrain into the diffusion flame resulting in flame suppression.

4. CONCLUSIONS

Efficient design of water-mist systems aims at obtaining the maximum amount of suppression for the minimum amount of water-mist added to the system. Numerical simulations have been described for optimizing the various mist injection characteristics for maximum flame suppression. The role of droplet diameter, injection angle (throw angle), mist density and velocity on entrainment and overall flame suppression is investigated using a two-continuum, time dependent Eulerian model. The net suppression ($\Delta H_T/\Delta H_o$) for various water-mist injection configurations (discussed in the Results and Discussion section) has been shown in Figure 14 as a function of mist to fuel flow rate ration. Both symmetric and asymmetric spray pattern geometries are considered. This figure clearly illustrates that net flame suppression is a function of various water-mist injection characteristics. The goal of this study has been to optimize these injection characteristics to obtain the maximum flame suppression for the minimum water-mist to fuel flow rate ratio. The main conclusions derived from this study can be summarized as follows:

- Under base injection configuration, the water-mist to fuel flow rate ratio required for extinguishment reduces with decreasing droplet size. The ratio of mist to fuel flow rate ($\dot{m}_{mist}/\dot{m}_{fuel}$) required for extinction is approximately 40 for 150 μ m droplets and reduces to 10 for 50 μ m

diameter droplets. Flame suppression increases with higher injection density or lower mist velocity for a given flow rate and droplet diameter.

- Under base injection configuration, net suppression reduces as the spray injection velocity increases (or spray injection density decreases) for a given mist to fuel flow rate ratio. Smaller droplet diameters produces maximum suppression for the minimum spray injection density.
- Under symmetric injection (base injection of water-mist directed at 45° angle) smaller diameter droplets produce more flame suppression. In contrast, under asymmetric injection, larger diameter droplets produce more flame suppression.
- Asymmetric mist injection can significantly alter the flame structure and flow field. In general asymmetric conditions produce lower suppression even with higher injection densities as compared to the symmetric case.
- Mist injection velocities close to the inlet gas velocity result in net suppression that is nearly independent of injection angle.
- Asymmetric mist injection show an optimum suppression angle of 45° .
- In contrast with base injection, side injection configuration clearly shows that larger diameter droplets produce more flame suppression. Under side injection configuration flame suppression increases with smaller mist density or higher injection velocity for a given flow rate and droplet diameter.

The generality of these conclusions for other flames/fires is currently being investigated. The following additional studies are being conducted to obtain a detailed understanding of the physical process involved during the interaction of water-mist and flames. These results will be presented in subsequent reports.

- Numerical models are being developed to simulate the burning rates of two-dimensional or axisymmetric liquid (methanol or heptane) pool fires. An energy equation is solved in the liquid pool and is coupled with the gas phase equations through appropriate interphase conditions. A Clausius-Clapeyron relationship is used to obtain the burning rates of the liquid pool.
- The temperature profiles above a liquid pool are being compared with experimental data obtained over a similar geometry. The burning rates of liquid pool fires is also being compared with experimental data available in the literature.
- The effect of the various water-mist injection characteristics (base injection, side injection or top injection) on overall flame suppression is being investigated for methanol pool fires.
- The changes in pool burning rates as a function of the various water-mist injection characteristics is being studied.

5. ACKNOWLEDGEMENT

The work described in this report was performed by the Laboratory for Computational Physics and Fluid Dynamics of the Materials Science and Component Technology Directorate, Naval Research Laboratory. The work was funded by the Office of Naval Research, Code 334, under the Damage Control Task of the FY97 BA2 Surface Ship Hull, Mechanical and Electrical Technology Program (PE0602121N).

6. REFERENCES

1. Evans, D.D. and Pfenning, D., *Oil and Gas Journal*, 8, pp. 80-86, (1985).
2. McCaffrey, B.J., *Comb. Sci. & Tech.*, 40, pp. 107-136, (1984).
3. Mawhinney, J. R., Dlugogorski, B. Z., Kim, A. K., *4th Int. Sym. on Fire Safety Sciences*, (1994).
4. Holmsted, G. *International Conference on Water Mist Fire Suppression Systems* (1993).
5. Rashbash, D.J., *Fire Safety Science*, pp. 1145-1163, (1986).
6. Tatem, P.A., Beyler, C.L., DiNunno, P.J., Budnick, E.K., Back, G.G. and Younis, S.E., *NRL Memorandum Report*, NRL/MR/6180-94-7624, (1994).
7. Tamanini, F., *Comb. Sci. & Tech.*, 14, pp. 17-23, (1976).
8. Downie, B., Polymeropoulos C. and Gogos, G., *Fire Safety Journal*, 24, pp. 359-381, (1995).
9. Beyler, C.L., *Journal of Fire Protection Engineering*, 4, pp. 5-16, (1992).
10. Seshadri, K., *Combust. Flame*, 33, pp. 197-215 (1978).
11. Mell, W.E., Baum, H.R. and McGratten, K., *2nd International Conference on Fire Research and Engineering*, (1997).
12. Nam, S., *Annual Conference on Fire Research*, (1996).
13. Lentati, A.M. and Chelliah, H.K., *Proceedings of the Fall Technical Meeting*, The Eastern States Section of the Combustion Institute, p. 281, (1996).
14. Chen, N.H., Rogg, B., and Bray, K.N.C., *Twenty-fourth Symposium (International) on Combustion*, The Combustion Institute, pp. 1513-1521, (1992).
15. Atreya, A., Crompton, T. and Suh, J., *NIST Annual Conference for Fire Research*, NISTIR 5499, pp. 67, (1994).
16. Hoffman, N.A. and Galea, E. R., *Int. J. Heat Mass Transfer*, Vol. 36, No. 6, pp. 1435, (1993).
17. Hoffman, N.A. and Galea, E. R., *Int. J. Heat Mass Transfer*, Vol. 36, No. 6, pp. 1445, (1993).
18. Prasad, K., Li, C., Kailasanath, K., Ndubizu, C., Gopal, R. and Tatem, P.A., *Comb. Sci. & Tech.*, accepted for publication, (1997).
19. Prasad, K., Li, C., Kailasanath, K., Ndubizu, C., Gopal, R. and Tatem, P.A., *Naval Research Laboratory*, NRL/MR/6410-97-8102 (1997).
20. Westbrook, C. K. and Dryer, F. L., *Comb. Sci. & Tech.*, Vol. 27, pp. 31-43, (1981).
21. Kailasanath, K., Oran, E.S. and Boris, J.P., *NRL Memorandum Report*, 4910, (1982).
22. Sirignano, W.A., *Prog. Energy Combust. Sci.*, Vol. 9, pp. 291-323, (1989).
23. Faeth, G.M., *Prog. Energy Combust. Sci.*, Vol. 3, pp. 191-224, (1977).
24. Tambour, Y., *Combust. Flame*, 58:103-114, (1984).
25. Prasad, K., Li, C. and Kailasanath, K., *27th Symposium International on Combustion*, (1998).
26. Patnaik, G., Laskey, K.J., Kailasanath, K., Oran, E.S. and Brun, T.A., *NRL Memorandum Report*, 6555, (1989).
27. Boris, J.P., and Book, D.L., *Methods in Computational Physics*, 16:85-129, (1976).

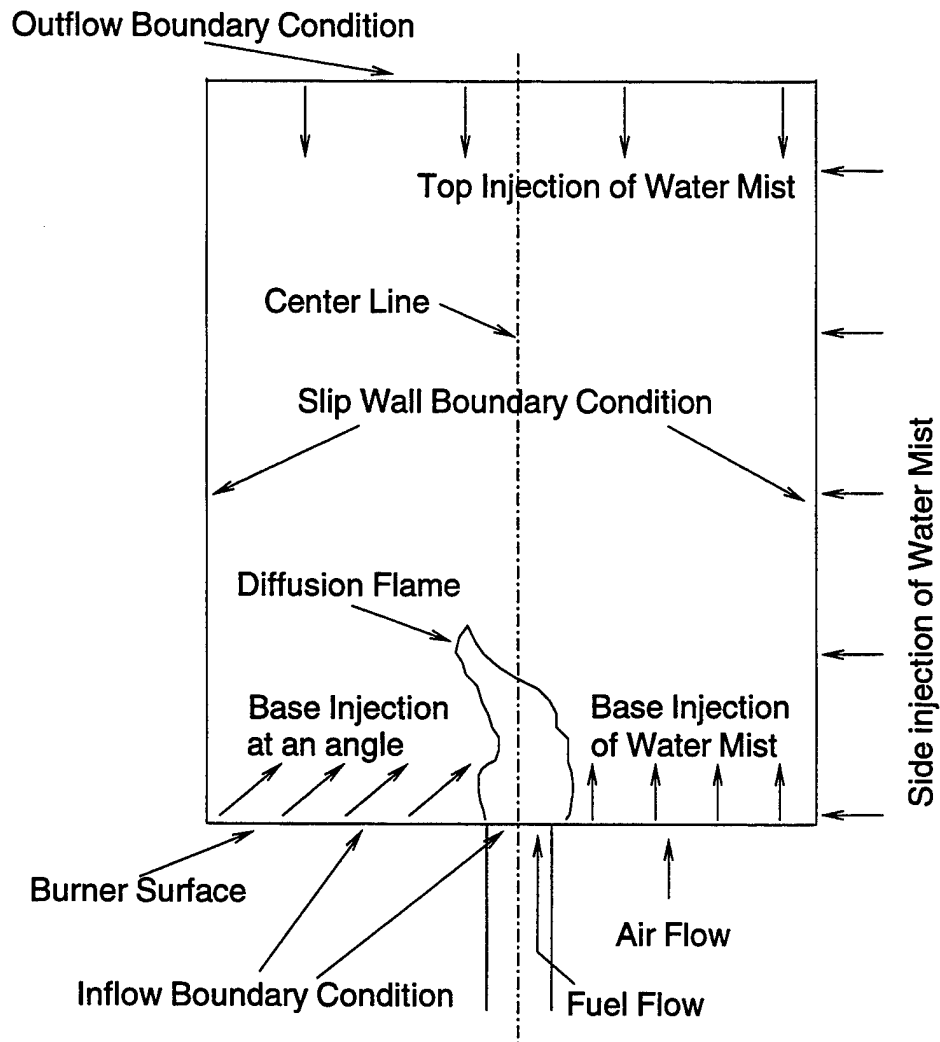


Fig. 1. Schematic diagram of a 2-Dimensional diffusion flame burner and the associated computational domain in which the solutions are desired. The figure also shows the various water-mist injection configurations that are studied in this report.

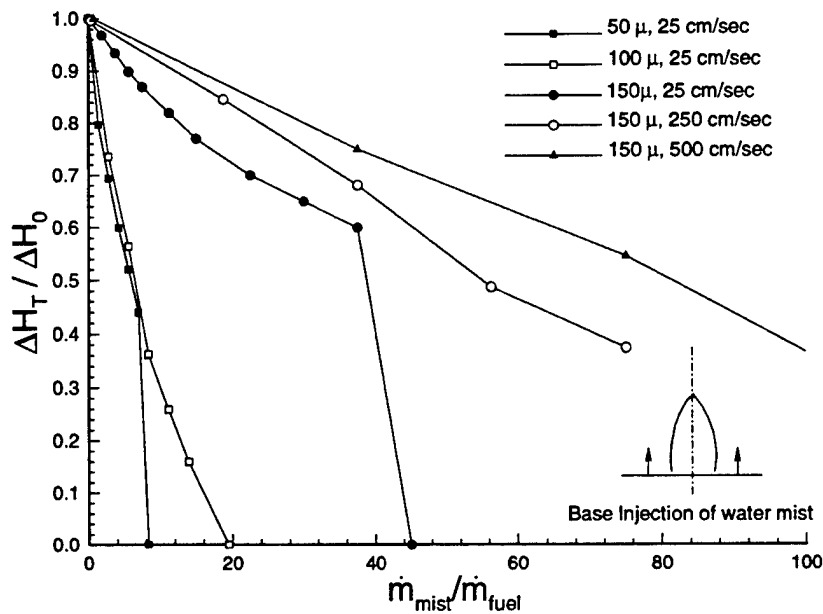


Fig. 2. The effect of droplet injection diameter and injection velocity on overall flame suppression is shown as a function of mist to fuel flow rate. The arrows in the insert indicate the direction in which water-mist is injected.

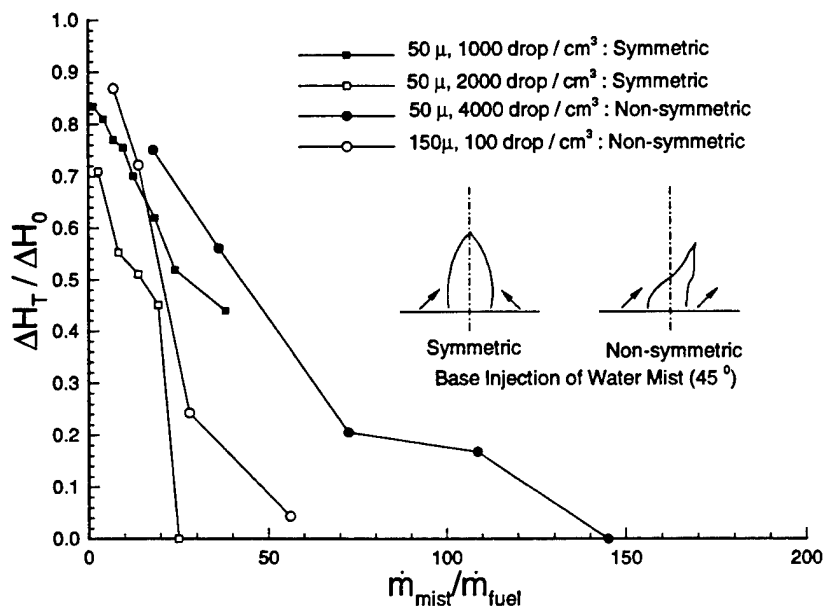


Fig. 3. The effect of droplet injection density and spray pattern (symmetric or asymmetric injection) on overall flame suppression shown as a function of mist to fuel flow rate. The arrows in the inserts indicate the direction in which water-mist is injected.

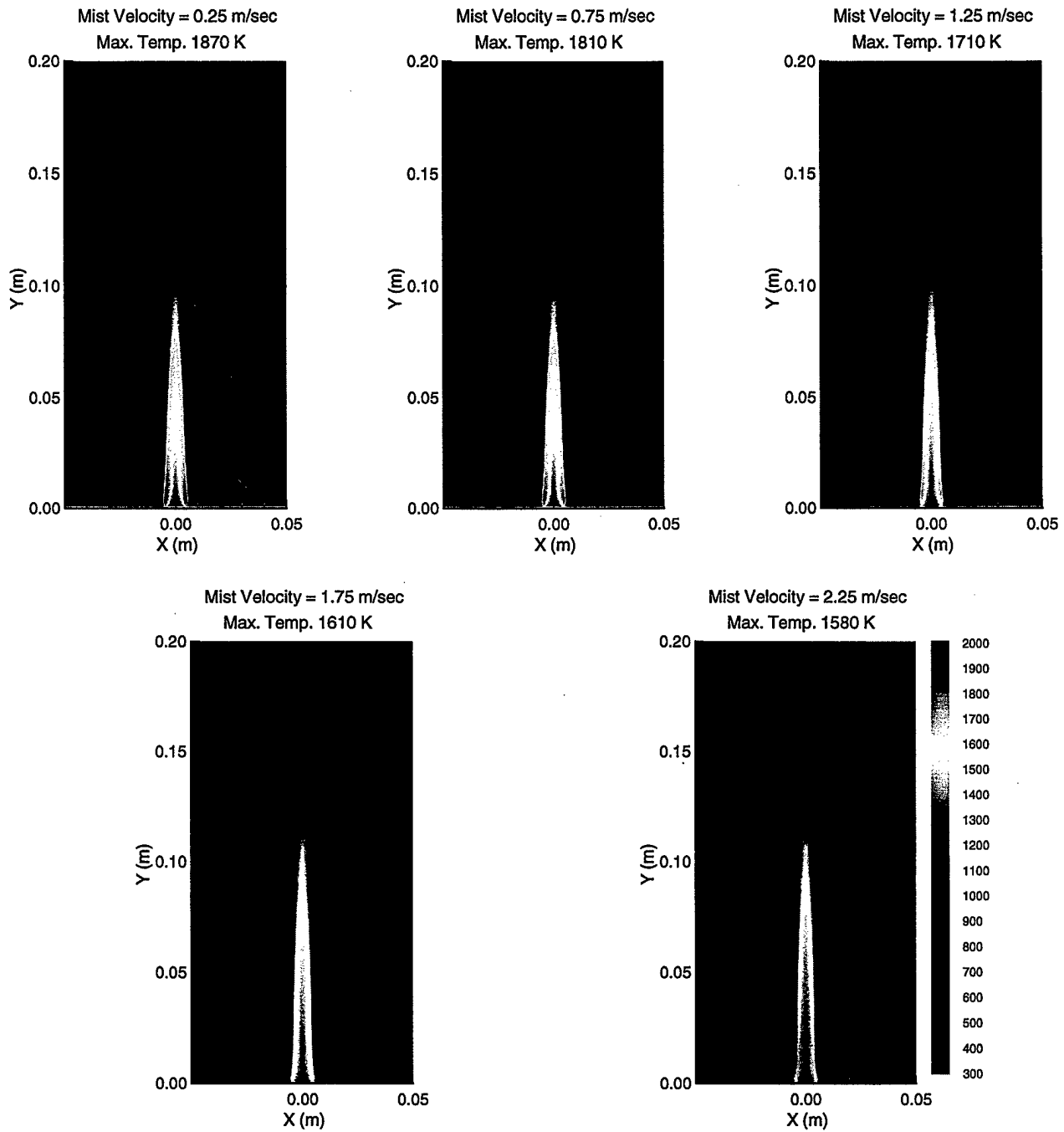
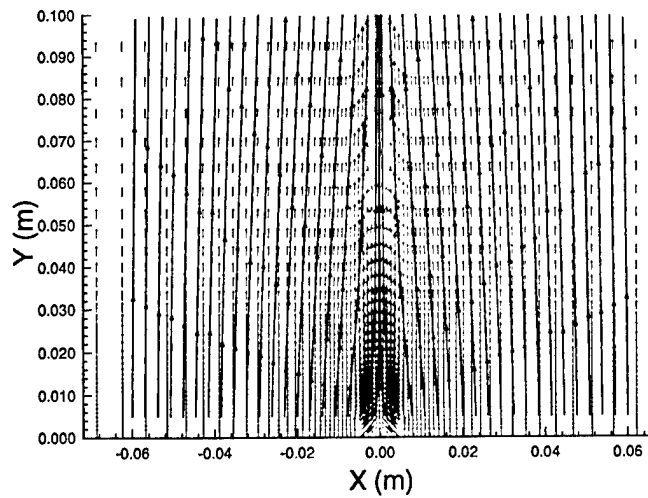
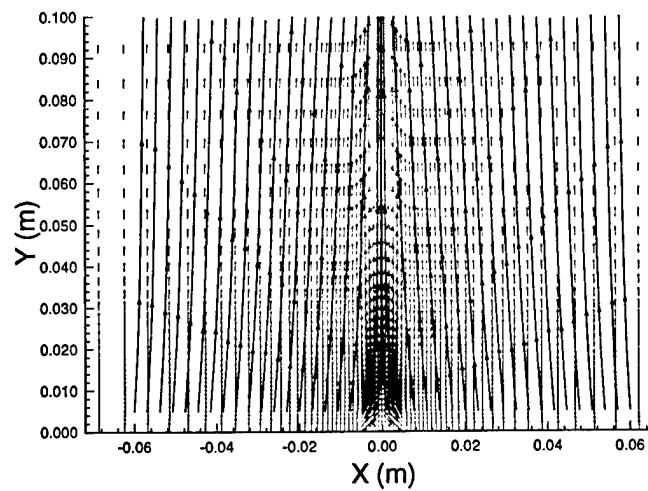


Fig. 4. The effect of varying the mist injection velocity on the temperature distribution for asymmetric mist injection at 45° angle to the air co-flow. The initial droplet diameter is 50μ and the injection density is $1000\text{drops}/\text{cm}^3$. The mist injection velocity is varied from $0.25\text{m}/\text{s}$ to $2.25\text{m}/\text{s}$.

a). Mist Velocity = 0.25 m/s



b). Mist Velocity = 1.25 m/s



c). Mist Velocity = 2.25 m/s

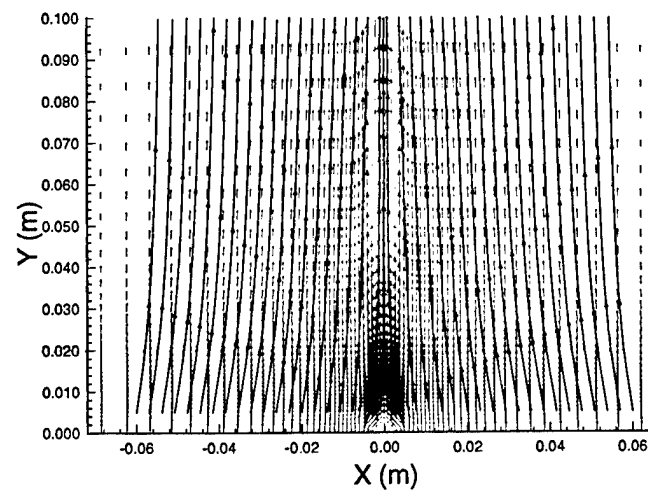


Fig. 5. Velocity vectors and streamline pattern during symmetric injection of water-mist at 45° angle to the air co-flow. The mist injection velocity is varied 0.25 m/s(top) to 2.25 m/s(bottom).

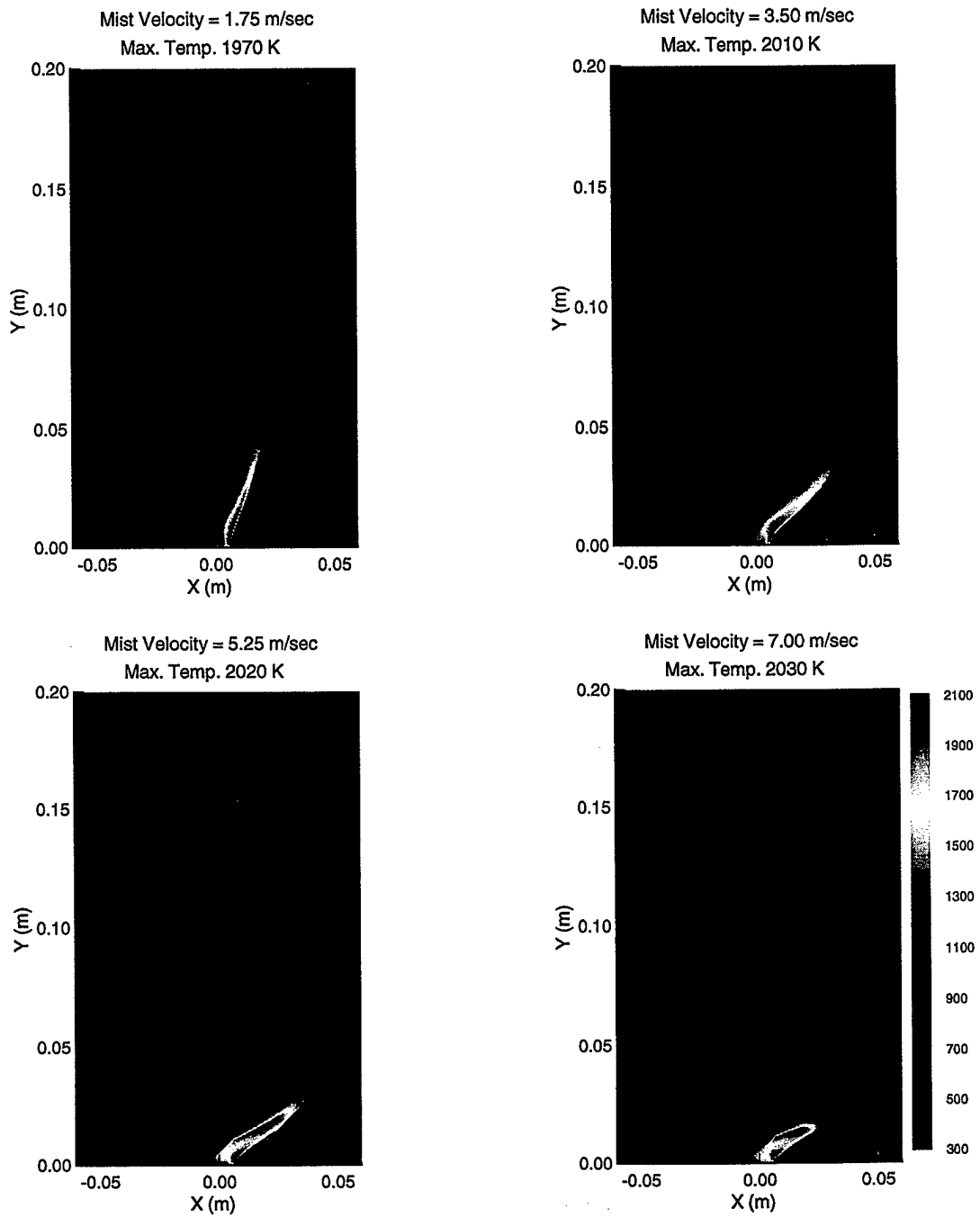


Fig. 6. Temperature contours for the asymmetric injection configuration of water-mist at 45° angle to the air co-flow. The water-mist droplet diameter is 50μ and the injection density is 4000 drops/cm^3 . The mist injection velocity is varied from 1.75m/s to 7.00m/s .

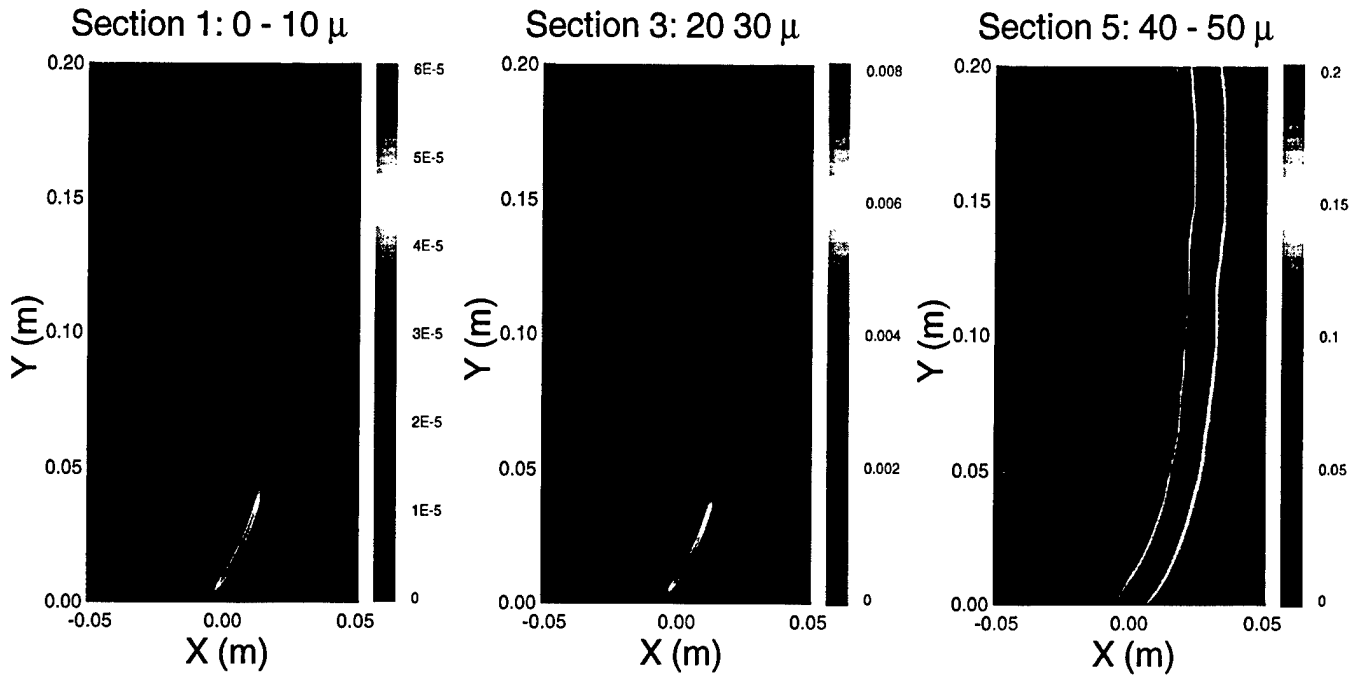


Fig. 7. Sectional density contours above a methane-air diffusion flame burner for asymmetrical injection of water-mist at 45° angle. The water-mist droplet diameter is 50μ , injection density is 4000 drops/cm^3 and mist injection velocity is 1.75 m/s .

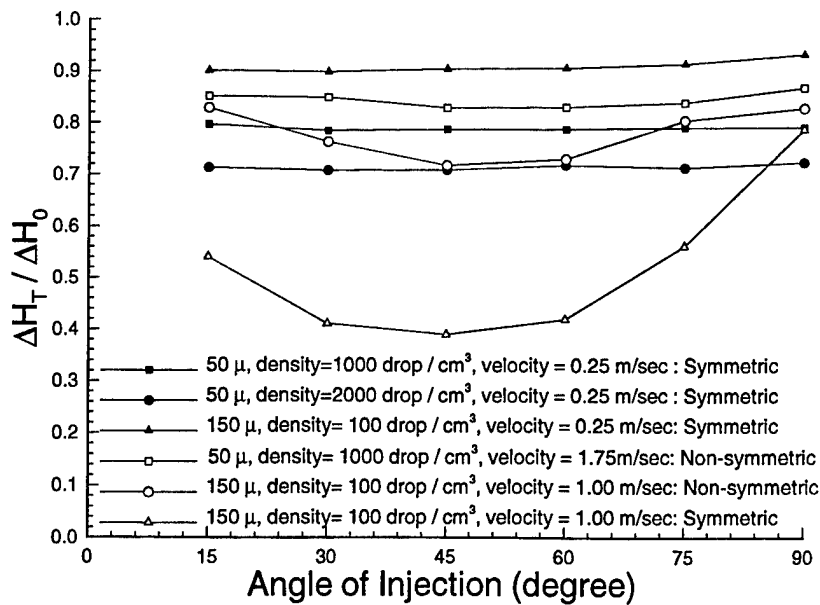


Fig. 8. Net suppression effect of water-mist as a function of injection angle. Both symmetric and asymmetric base injection configurations are considered.

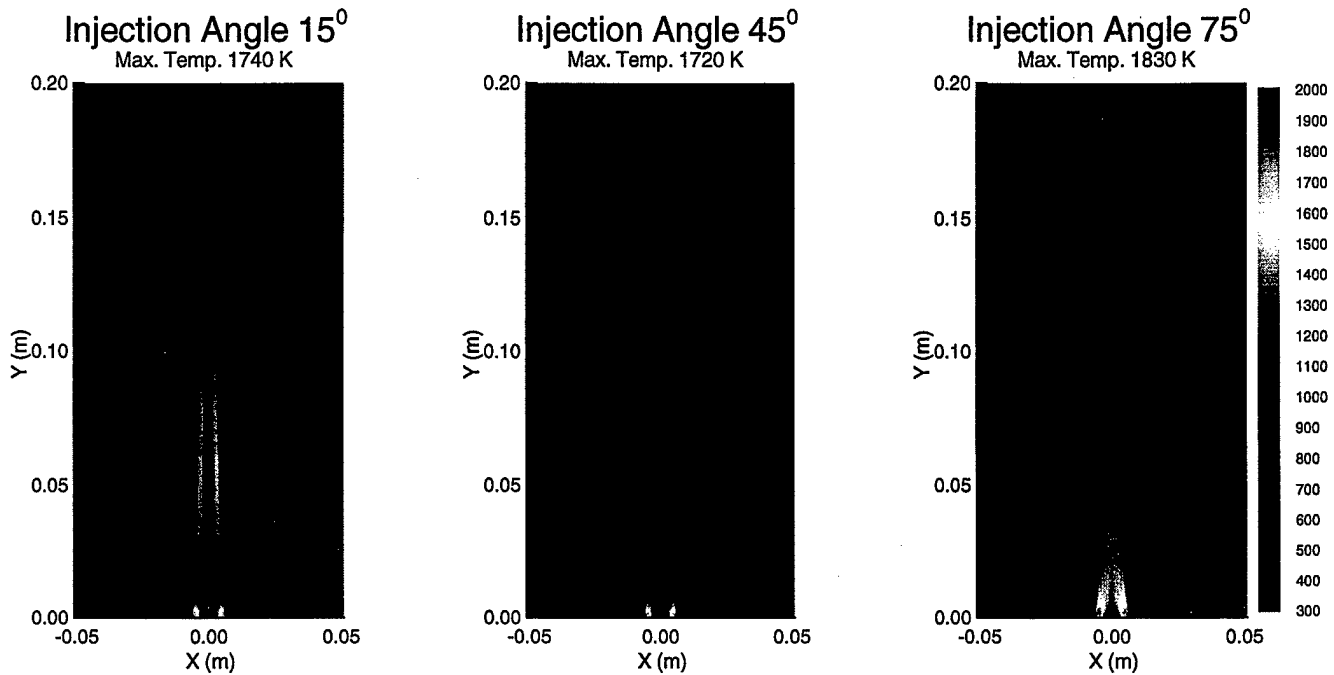


Fig. 9. Temperature contours during symmetric injection configuration of water-mist at various injection angles. Droplet diameter is 150μ , injection density = $100 \text{ drop}/\text{cm}^3$ and injection velocity = $1.00\text{m}/\text{s}$.

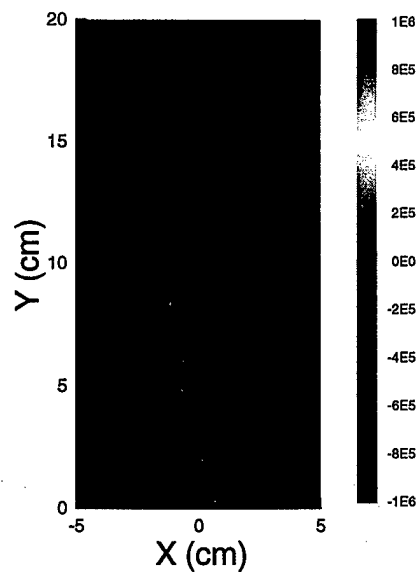


Fig. 10. Heat release rate contours ($\text{J}/\text{m}^3/\text{s}$) during side injection of water-mist. Figure shows the exothermic contours (red) at the flame sheet due to oxidation of the fuel molecule, and endothermic contours (blue) due to evaporation of water droplets.

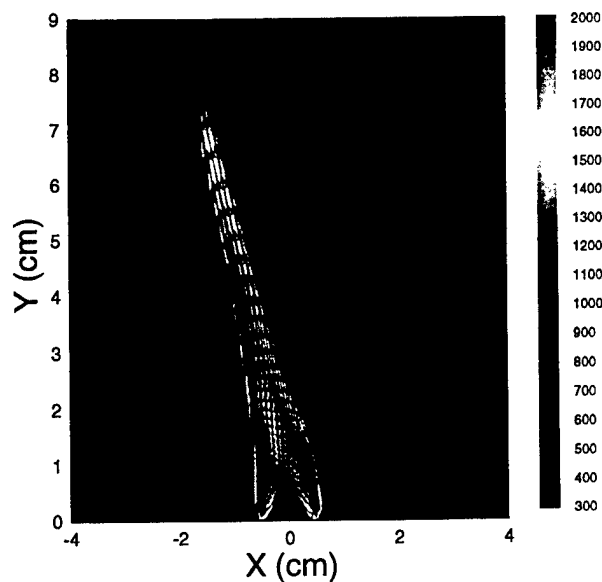


Fig. 11. Velocity vectors (m/s) superimposed on temperature (K) distributions during side injection of water-mist into a methane-air diffusion flame.

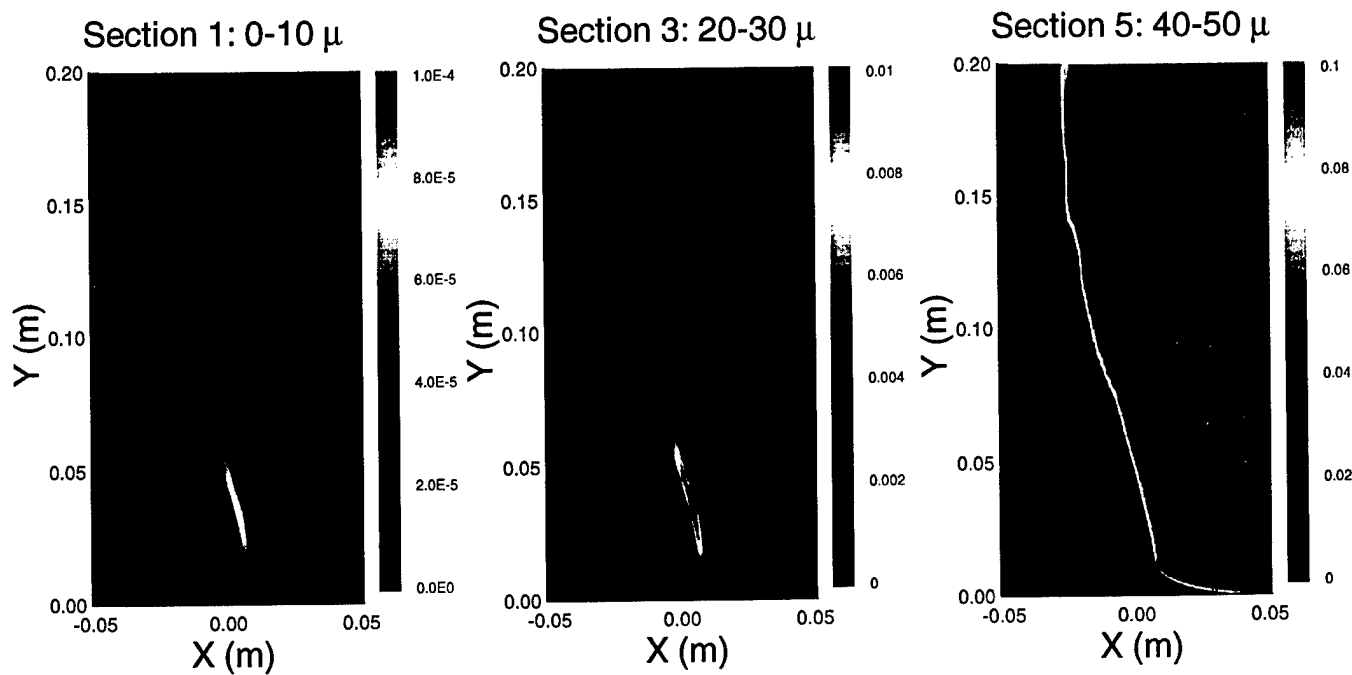


Fig. 12. Sectional density contours above a methane-air diffusion flame burner for side injection of water-mist. The water-mist droplet diameter is 50μ , injection density is $2000 \text{ drops}/\text{cm}^3$ and mist injection velocity is $12.5\text{m}/\text{s}$.

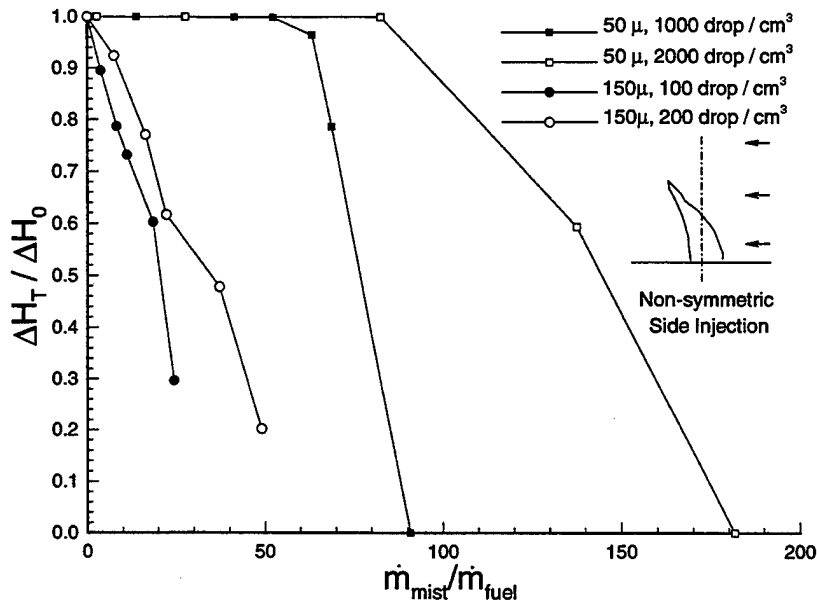
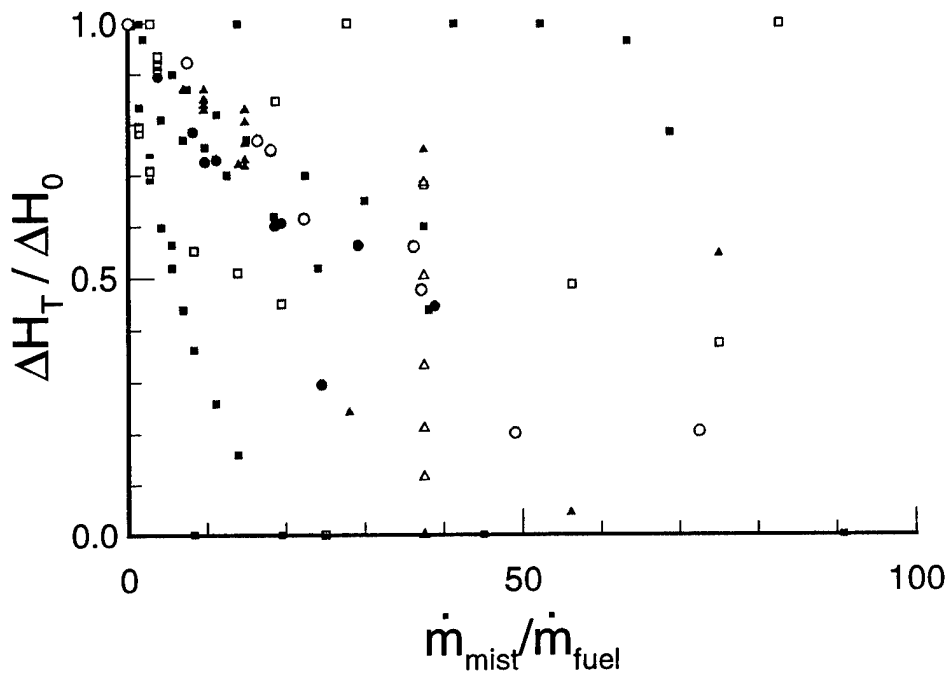


Fig. 13. Net suppression effect of water-mist as a function of mist to fuel flow rate ratio for side injection configuration. The effect of droplet diameter on overall flame suppression has been shown for (asymmetric) diffusion flames. The arrows in the insert indicate the direction in which water-mist is injected.



Symmetric Injection

Non-symmetric Inj.

- | | |
|--------------------------------------------------|-------------------------------------------------|
| ■ 50 μ , $mv=0.25$ m/sec | ● 50 μ , 1000 d/cm ³ , 45° |
| ■ 100 μ , $mv=0.25$ m/sec | ○ 50 μ , 4000 d/cm ³ , 45° |
| ■ 150 μ , $mv=0.25$ m/sec | ▲ 150 μ , 100 d/cm ³ , 45° |
| □ 150 μ , $mv=2.5$ m/sec | ▲ 50 μ , 1000 d/cm ³ , 1.7 m/sec |
| ▲ 150 μ , $mv=5.0$ m/sec | ▲ 150 μ , 100 d/cm ³ , 1.0 m/sec |
| □ 50 μ , 1000 d/cm ³ , 0.25 m/sec | ■ 50 μ , 1000 d/cm ³ , SI |
| 50 μ , 2000 d/cm ³ , 0.25m/sec | □ 50 μ , 2000 d/cm ³ , SI |
| □ 150 μ , 100 d/cm ³ , 0.25 m/sec | ● 150 μ , 100 d/cm ³ , SI |
| ▲ 150 μ , 100 d/cm ³ , 2.5 m/sec | ○ 150 μ , 200 d/cm ³ , SI |
| ■ 50 μ , 1000 d/cm ³ , 45° | |
| □ 50 μ , 2000 d/cm ³ , 45° | |
| 150 μ , 100 d/cm ³ , 45° | |

Net Suppression of CH₄ - Air Diffusion Flames

Fig. 14. Net suppression effect of water-mist as a function of mist to fuel flow rate ratio for various injection configuration and spray pattern geometries.